

Article

A Study on the Pore Structure and Fractal Characteristics of Briquettes with Different Compression Loads

Lingling Qi^{1,2,3,4} , Xiaoqing Zhou¹, Xinshan Peng^{1,*} , Xiangjun Chen^{1,2,3,4}, Zhaofeng Wang^{1,2,3,4} and Juhua Dai¹

¹ School of Safety Science and Engineering, Henan Polytechnic University, Jiaozuo 454099, China

² MOE Engineering Research Center of Coal Mine Disaster Prevention and Emergency Rescue, Jiaozuo 454099, China

³ Collaborative Innovation Center of Coal Work Safety and Clean High Efficiency Utilization, Jiaozuo 454003, China

⁴ State Key Laboratory Cultivation Base for Gas Geology and Gas Control, Jiaozuo 454099, China

* Correspondence: peng5207@126.com

Abstract: In order to study the effects of different compression loads on the pore characteristics of coal, taking remolded coal as the research object, the mercury intrusion method was used to determine the pore structures of the briquettes under the compression loads of 50, 70, 90 and 110 MPa, and the Menger sponge model was used to conduct fractal research on the measured parameters. The results show that the compression load has a significant effect on the pore structure parameters of the briquettes. The hysteresis loop generated by the mercury-intrusion and mercury-extrusion curves of raw coal is small, and the pore connectivity is better. After different loads are applied for briquettes, the hysteresis loop becomes larger, and the pore connectivity becomes worse. From the process of the raw coal to the briquettes loaded at 50 and 70 MPa, the pore-specific surface area reduced from 5.069 m²/g to 1.259 m²/g, the total pore volume increased from 0.0553 cm³/g to 0.1877 cm³/g, and the average pore size increased from 43.6 nm to 596.3 nm. When the compression load reached 70 MPa, the specific surface area, total pore volume, and average pore diameter of briquettes remained basically stable with the change in the compression load. The micropores and visible pores and fissures of raw coal contribute 78% of the pore volume, and the micropores and minipores contribute 99% of the specific surface area. After being pressed into briquettes, the volume of mesopores and macropores increases, the volume of visible pores and fractures decreases and the volume of minipores changes little; additionally, the pore surface area contributed by mesopores and macropores increases, and the pore surface area contributed by micropores decreases, indicating that the effect of compression load on pores of 10–100 nm is not obvious, mainly concentrated in the 100–10,000 nm region. The fractal curve of briquettes is fitted into three sections, which are defined as low-pressure sections 1 and 2 and high-pressure section 3, and the fractal dimensions are D₁, D₂ and D₃ respectively. The fractal dimension D₁ of briquettes with different compression loads is close to 2, D₂ is close to 3 and D₃ is greater than 3. The pore structures of briquettes have obvious fractal characteristics in the low-pressure sections 1 and 2 but do not conform to the fractal law in the high-pressure section. Furthermore, in the micropore stage of briquettes, the measured surface area and volume are both negative, indicating that the mercury intrusion method used to test the pore structure of the loaded briquette is more likely to cause the collapse of and damage to the pores in the micropore (<10 nm) stage.

Keywords: briquette; load; pore structure; fractal dimension; mercury intrusion method



Citation: Qi, L.; Zhou, X.; Peng, X.; Chen, X.; Wang, Z.; Dai, J. A Study on the Pore Structure and Fractal Characteristics of Briquettes with Different Compression Loads. *Sustainability* **2022**, *14*, 12148. <https://doi.org/10.3390/su141912148>

Academic Editors: Danqi Li, Ping Chang, Saisai Wu, Jianhang Chen and Chaolin Zhang

Received: 17 August 2022

Accepted: 21 September 2022

Published: 26 September 2022

Publisher's Note: MDPI stays neutral with regard to jurisdictional claims in published maps and institutional affiliations.



Copyright: © 2022 by the authors. Licensee MDPI, Basel, Switzerland. This article is an open access article distributed under the terms and conditions of the Creative Commons Attribution (CC BY) license (<https://creativecommons.org/licenses/by/4.0/>).

1. Introduction

Disasters such as coal and gas outbursts are still the main disasters that endanger safety in coal mines. Scholars have conducted a great deal of in-depth research and practice

on the prevention of outbursts and have achieved relatively significant results. However, outburst disaster accidents still occur from time to time in recent years [1,2]. Coal mine disasters mainly occur in geological tectonic belts and areas of rock cross-cut coal, where the original structure of the coal body in the geological structure belt and the coal body in the area of rock cross-cut coal that has been pre-drained will be seriously damaged, and the strength is low; therefore, it is difficult to drill the columnar raw coal on site. Even when the samples are prepared, they are still single samples in the coal seam that are not typical or representative of the actual geological tectonic belts and the area of rock cross-cut coal [3,4]. Furthermore, the high heterogeneity of coal sometimes makes it difficult to interpret the results of laboratory experiments. Therefore, more homogeneous samples with reproducible characteristics in the laboratory will provide some key advantages [5,6]. Coal samples of similar materials can be obtained by pressing pulverized coal particles under certain conditions, and it is possible to use briquettes to carry out relevant experimental research from the previous research experience. Previous researchers used briquettes as the experimental sample and made some progress in infiltration [7–10], freezing [11–13], adsorption and desorption [14–16], gas outburst [17,18], etc. Jia et al. [9] studied the response characteristics of permeability to stress by taking raw coal samples and briquette samples as research objects and found that it was feasible to use briquette samples instead of raw coal samples to study the seepage characteristics of gas-containing coal; this also had certain advantages in some specific occasions. Gan et al. [19] used a new method of heating briquette samples to study the effect of heating temperature on the strength, porosity, and fracture structure of briquettes and concluded that with the increase in heating temperature, the pore volume, specific surface area; average pore diameter of the briquette samples first decreased and then increased; the smooth and complete layered structure transformed into a rough fractured layered structure; and the pores changed from indistinct micropores to observable mesopores and macropores and determined the appropriate heating temperature for the briquette forming process. Zhao et al. [20] studied the structural characteristics of carbonized anthracite briquettes obtained at different pyrolysis temperatures and found that the pyrolysis of anthracite briquettes mainly includes three processes: drying, decomposition, and binding–re-polymerization. Norbert et al. [21] prepared briquettes with porosity ranging from 13.5% to 33% and analyzed the mechanical and gas properties of the briquette, and they determined that the changes in the porosity of the briquettes allowed for obtaining coal materials with parameters typical of in situ coal; additionally, the mechanical and gas properties of briquette made them amenable to representative outstanding studies. Li et al. [22] selected samples of medium coal rank from Xinjiang mines, prepared four kinds of briquette samples with different particle sizes and studied the pore structure characteristics, gas adsorption characteristics and their correlations of briquette under different particle size conditions. They found that the peak areas of the medium and large pores and the total pore spectra were negatively correlated with the particle size of the briquette, the peak area of the micropore spectrum was positively correlated with the particle size and the smaller the average particle size of the briquette, the greater the total amount of adsorbed gas. Xu et al. [23] used briquettes made from coal with different particle sizes and used analysis software to study the pore structure of the briquette, and they found that as the particle size of the briquettes gradually decreased, the radius of the briquette pores gradually decreased, the total number of pores increased, the fractal dimension increased the degree of pore development increased and the degree of uniformity of pore distribution increased gradually. Pores in coal are the storage sites and migration channels of coal seam gas, and the characteristics of pore structure directly affect the migration and enrichment of coal seam gas [24,25]. Accurate and quantitative description of coal pore structure characteristics is important for understanding coal seam gas occurrence state, gas desorption, diffusion and seepage, gas drainage and other indicators [26–29].

It is necessary to study the influence of different forming conditions on the characteristics of briquettes. Prior researchers have studied the pore characteristics of briquettes of different particle sizes, but there are few studies on the pore structure characteristics of

briquettes under different compression loads. Therefore, in this paper, the pore structure of briquette is tested with mercury intrusion experiments, and the fractal laws are obtained by combining fractal theory analysis; pore structure characteristics are characterized. This study is expected to provide a theoretical basis for laboratory research on briquettes and to lay a foundation for the study of gas migration characteristics in coal.

2. Materials and Methods

2.1. Sample Collection and Processing

The experimental coal samples are taken from the fresh coal samples of the 3514 working face of No. 3 coal seam in Yonghong Coal Mine, and the coal rank is anthracite. The coal sample preparation steps are as follows:

(1) Crush the obtained fresh coal samples and select two coal samples, of particle sizes 0.25–0.50 mm and below 0.25 mm, for the production of reshaped coal bodies (shown in Figure 1a,b). The raw coal is used for comparative experiments.

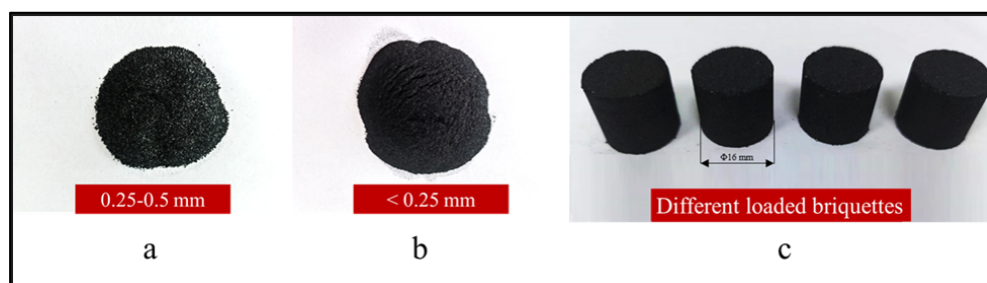


Figure 1. The processing and production of briquettes.

(2) Put the two coal samples screened above into a 105 °C drying oven for 12 h. After the dried coal samples are cooled to room temperature in the laboratory, the coal samples with particle sizes of 0.25–0.50 mm and below 0.25 mm are weighed according to the ratio of 1:2, a certain mass is weighed and 10% distilled water is added to stir well.

(3) Put the fully stirred wet coal sample into the briquette mold embedded with an inner tube, and use an EHC-3100 microcomputer-controlled electro-hydraulic servo universal machine to press the experimental coal.

(4) Set the compression load for 50 MPa and hold the pressure for 0.5 h.

(5) Turn the mold upside down, and then use the servo universal testing machine to withdraw the reshape coal safely and slowly to make a briquette sample with a $\phi 16$ mm and a height of 16 mm for mercury intrusion experiments (shown in Figure 1c).

(6) The briquette samples are dried in a drying oven for 12 h, and the drying oven temperature is set to 105 °C.

(7) Change the compression load in step (4) to 70, 90, and 110 MPa in turn, and repeat steps (5)–(6)

2.2. Experimental Method

Mercury intrusion is widely used when testing the structures of pores and fissures in porous media. The method is to inject liquid mercury into the pores and fissures of the coal sample through external pressure. The greater the external mercury injection pressure, the smaller the effective width of the liquid mercury that can be pressed into the pores and cracks of the coal. Therefore, a specific pressure corresponds to a specific effective width of cracks and fissures, and the corresponding amount of injected mercury is equal to the volume of pores and fissures under the effective width. An Autopore IV9505 mercury porosimeter (made by Micromeritics of Norcross, Georgia, United States) is used in the mercury intrusion experiments in this paper. The experimental steps are as follows:

(1) Weigh the coal sample with an electronic balance with an accuracy of 0.0001 g and put the weighed coal sample into the sample tube.

(2) Install the tube containing the coal sample in the low-pressure station of the instrument for low-pressure analysis.

(3) After the low-pressure analysis, install the sample tube in the high-pressure station of the instrument and perform high-pressure analysis.

When mercury intrusion is used to analyze the pore structure, the commonly used B.B. Hodot pore classification method is followed: pores in the coals are classified as micropores (<10 nm), minipores (10–10² nm), mesopores (10²–10³ nm), macropores (10³–10⁵ nm) and visible pores and fissures (>10⁵ nm) [30].

3. Results and Discussion

3.1. Pore Characteristics of Briquette with Different Compression Loads

Wu et al. [31] used mercury intrusion–extrusion curves to characterize the pore morphology and connectivity of coal and divided the morphology into three types: open pores, transition pores and closed pores. The detailed mercury intrusion test curves are shown in Figure 2.

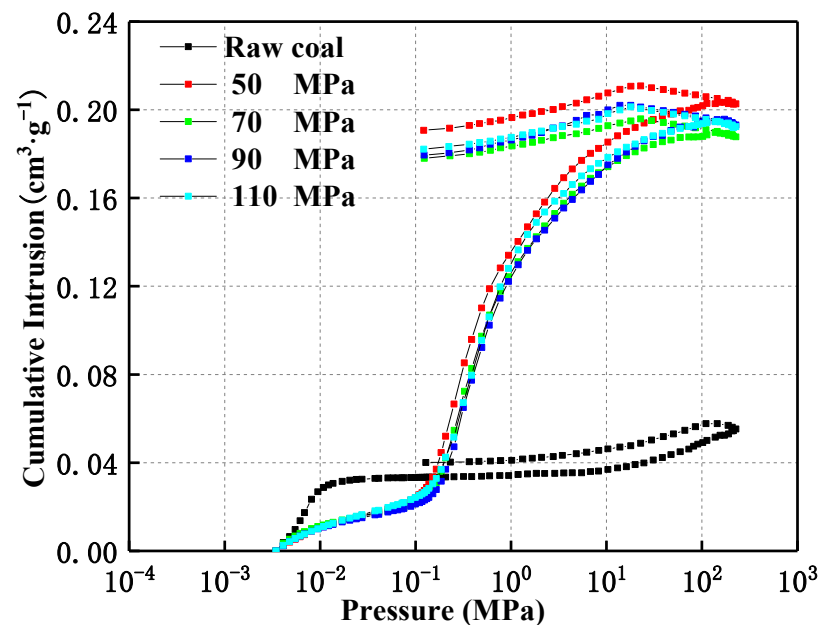


Figure 2. Mercury intrusion-extrusion curves of briquettes under different compression loads.

The mercury intrusion–extrusion curves of the coal samples constitute an obvious hysteresis loop that can be used to determine the pore type of coal. It can be seen from Figure 2 that the amount of mercury injected into the raw coal increases slightly when the pressure reaches 10^{−2} MPa; then, with increasing pressure, the amount of mercury intrusion tends to be flat, and there is no significant change. After the mercury injection pressure reaches 10 MPa, the mercury injection amount increases slightly, and the total mercury injection amount of the raw coal is generally less. The mercury intrusion–extrusion curves of the briquettes under the four different compression loads are basically the same. The mercury injection in the low-pressure area increases slowly, while the amount of mercury injected into briquettes increases sharply when the pressure reaches 0.1 MPa, and when the pressure reaches 100 MPa, the mercury injection curve shows a slow decrease again. In the process of applying loads of 50, 70, 90 and 110 MPa, the mercury intrusion–extrusion curves of briquettes are relatively consistent, and they are basically concentrated in the same area, indicating that the pore size distribution characteristics of briquettes under the load are basically the same. When the mercury injection pressure of raw coal is 10^{−2} MPa,

the corresponding pore width is 101,685 nm, and when the mercury injection pressure is 10 MPa, the corresponding pore width is 95.4 nm. Therefore, raw coal is mainly composed of intergranular pores, visible pores, fissures and micro-pores, with fewer mesopores and macropores. Under the action of the external load, the large pores of briquettes are compacted. When the mercury injection pressure is between 0.1 MPa and 100 MPa, the smaller pores in the briquettes with different compression loads increase more. After the mercury injection pressure is greater than 100 MPa, the excessive pressure causes serious damage to the pore structure of the briquettes, causing some pores to collapse. Compared with raw coal, the hysteresis loops of loaded briquettes are significantly larger than that of raw coal, showing that the pore connectivity of raw coal is better. Meanwhile, the difference between mercury intrusion and mercury extrusion becomes larger after higher loads are applied, and the hysteresis loop becomes larger, indicating that the pore connectivity of briquettes becomes worse under the action of external pressure. This is consistent with previous research [32,33].

The average pore size in the mercury intrusion method refers to the weighted average of the corresponding pore volumes of each pore size section. Figure 3 is the average pore size of briquettes with different compression loads; as the picture shows, the average pore size of the raw coal is smaller, and with increases in the applied load to 50 and 70 MPa, the average pore diameter of the briquettes increases linearly; the average pore diameter of the briquette under 110 MPa is basically the same as the briquette under 70 MPa. The average pore diameter of the briquette under 90 MPa is slightly smaller than those under 70 and 110 MPa, but they are all in the range of mesopores, which further shows that the applied load has a significant effect on the pore size distribution of briquettes under less than 70 MPa. The effect of the applied load on the average pore size of briquettes is weakened when the applied load is higher than 70 MPa. This is because the briquettes are pressed by pulverized coal under the action of external force, the intergranular pores cannot be completely compacted, and some pores in the coal are fractured by external force to generate new pores, so that the average pore size increases and then remains stable.

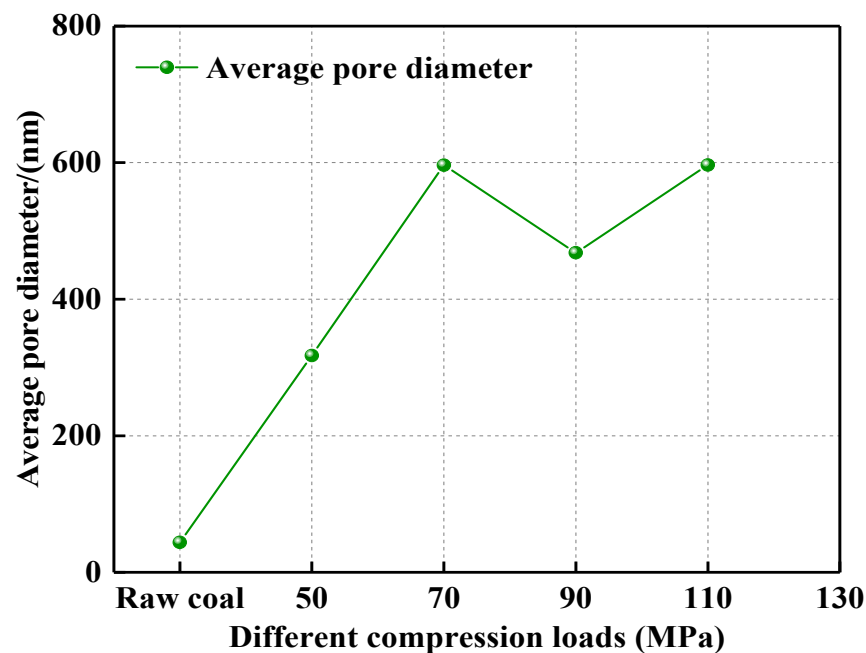


Figure 3. Average pore diameter of briquettes under different compression loads.

3.2. Pore Volume and Distribution of Briquette with Different Compression Loads

Figures 4 and 5 are the total pore volume and cumulative pore volume of briquettes with different compression loads, respectively. As shown in the figures, the pore volume of raw coal is small, and when the external load on the briquette is 50 MPa, the total pore volume is the largest. When the applied loads are 70, 90 and 110 MPa, the total pore volumes of the briquettes are basically the same, indicating that the greater the applied load, the more densely the intergranular pores of briquettes are compressed, and the total pore volume of the briquettes tends to be stable. Figure 6 shows the incremental pore volume distribution of briquettes under different compression loads, and Table 1 shows the pore volume distribution of briquettes under different compression loads. As can be seen from Figure 6, the pore volume peaks of raw coal are mainly concentrated in the range of pores diameters larger than 10,000 nm and smaller than 10 nm, and the rest of the diameter ranges have fewer peaks and little fluctuation. Under the action of external load, the peaks are distributed in each pore size range, and the maximum peak pore volumes under different compression loads of briquettes shift to the left and are mainly concentrated in the pore size range of 100–10,000 nm. It is further shown that the pore volume distribution of raw coal changes from “large at both ends and small in the middle” to “small at both ends and large in the middle” with the applied load, which destroys the original large-diameter pores in the coal sample and changes its pore volume distribution characteristics; the peak shifts are consistent with those of Zhang et al. [34,35]. It can be seen from Table 1 that the pore volume of raw coal is mainly contributed as minipores and visible pores and fissures; micropores, mesopores and macropores are all distributed but contribute less. With the increase in the external load of briquettes, compared with raw coal, the volume of visible pores and fissures in the briquettes decreases significantly, and the pore volume of mesopores and macropores increases greatly; the pore volume of the minipores also does not change much, while the micropores are destroyed and all volumes are negative. Visible pores and fissures are also destroyed, resulting in more mesopores and macropores, and the briquettes are compacted and become more dense. In the mercury intrusion test, with the increase of the mercury injection pressure, the micropore (<10 nm) volume in the loaded briquettes is destroyed, but the micropore (<10 nm) volume of the measured raw coal is intact, indicating that the external load has a great influence on the micropore (<10 nm) structure of briquettes, making the micropores (<10 nm) more fragile and brittle.

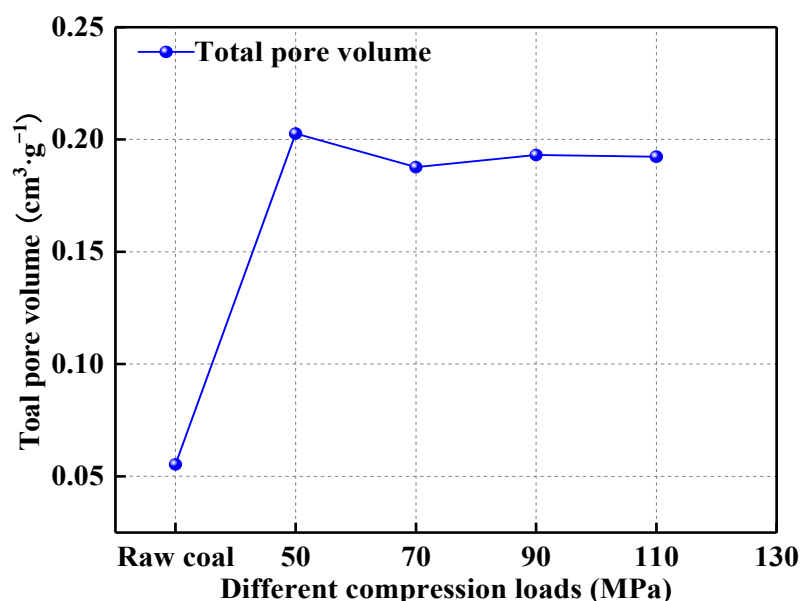


Figure 4. The total volume of briquettes under different compression loads.

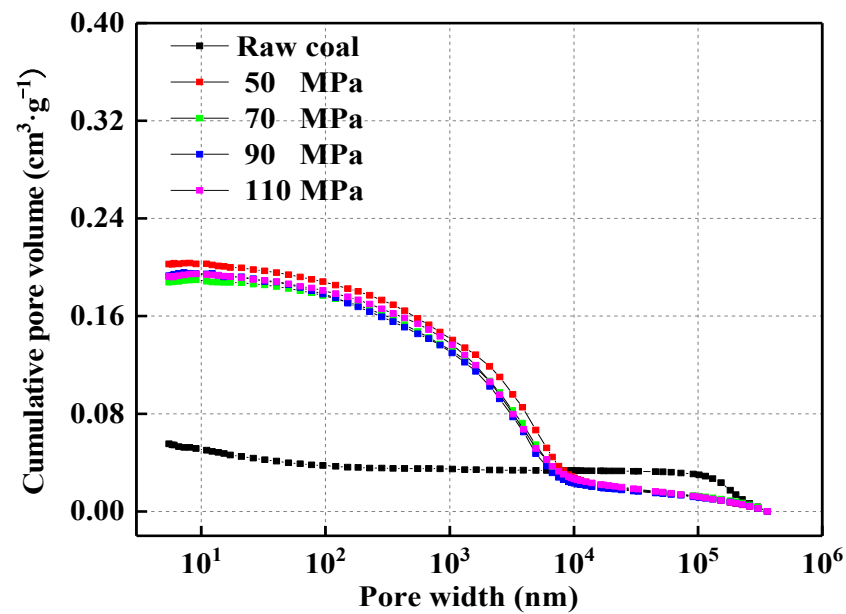


Figure 5. Cumulative pore volume of briquettes under different compression loads.

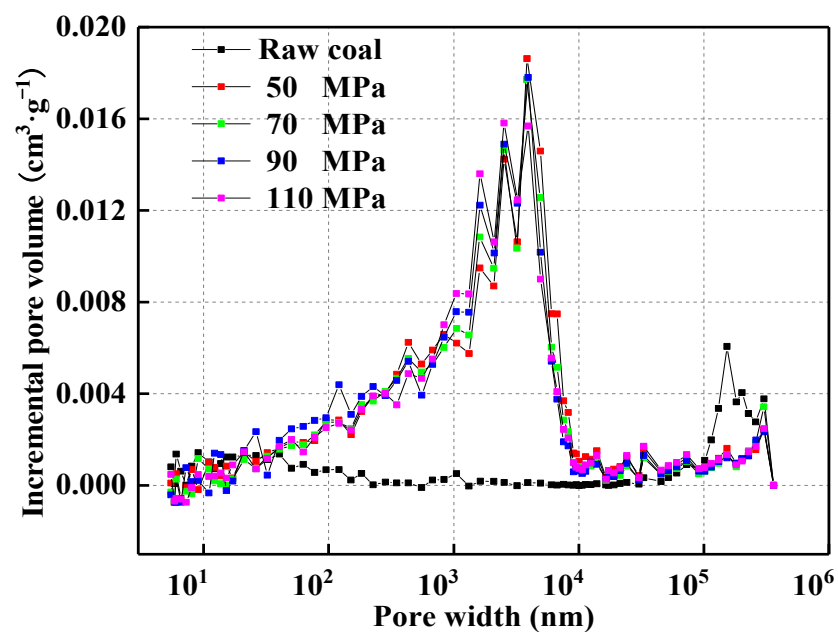


Figure 6. Incremental pore volume of briquettes under different compression loads.

Table 1. Pore volume distribution of briquettes under different compression loads.

Coal Sample	Pore Volume Distribution of Briquettes under Different Compression Loads (cm ³ ·g ⁻¹)				
	<10 nm	10–10 ² nm	10 ² –10 ³ nm	10 ³ –10 ⁵ nm	>10 ⁵ nm
Raw coal	0.0052	0.0132	0.0022	0.0048	0.0299
50 MPa	−0.003	0.0176	0.045	0.1285	0.0118
70 MPa	−0.0009	0.0145	0.043	0.1187	0.0124
90 MPa	−0.0015	0.0196	0.0453	0.1183	0.0114
110 MPa	−0.0018	0.0157	0.042	0.1246	0.0118

3.3. Pore Area and Distribution of Briquette with Different Compression Loads

Figures 7 and 8 are the specific surface area and cumulative pore area of briquettes with different compression loads, respectively. It can be seen from the figures that the specific surface area of raw coal is the largest, and the specific surface areas of the briquettes continue to decrease with the application of external load. When the applied loads are 70, 90, and 110 MPa, the specific surface area is basically stable. In the cumulative pore area diagram, the cumulative pore area changes little in the early stage and then gradually increases as the pore diameter of the loaded briquettes decreases. In the micropore stage, part of the micropore area is destroyed, and there is a certain degree of decline due to the excessive mercury pressure. Since the coal surface area is mainly provided by small size pores, there is a large cliff-like decline in the micropore stage in the cumulative pore area chart. According to the pore areas of briquettes under different compression loads in Figure 9 and the pore area distribution of briquettes under different compression loads in Table 2, it can be seen that the peak incremental pore area of raw coal is concentrated in pores smaller than 100 nm, and the peak incremental pore surface area of loaded briquettes is concentrated in pores of 10–100 nm, but the peak is significantly smaller. The surface area of raw coal is concentrated in the stage of micropore and minipore, while the micropore surface area of the loaded briquettes is destroyed; as a result, the surface area mainly comprises minipores and mesopores, and the surface area contributed by macropores also increases to a certain extent. When the applied load is greater than 70 MPa, the effect of the applied load on the specific surface area of briquettes is constant, and the specific surface area does not clearly change. Under the influence of the external load, the surface area of the micropores damaged by the excessive mercury injection pressure increases in an inverse proportion: With the continuous increase of the applied load, the damaged micropore surface area will tend to be stable.

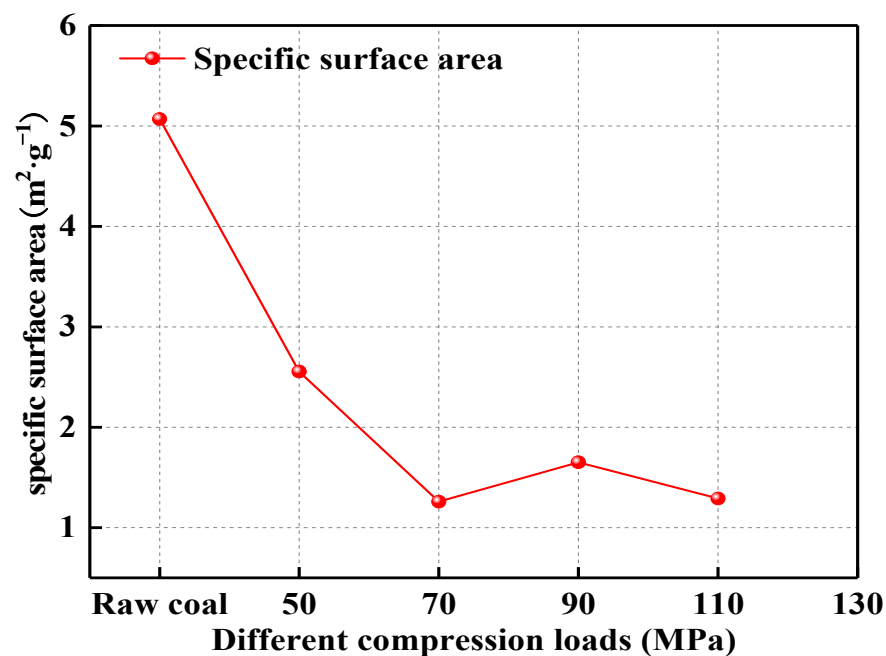


Figure 7. The specific surface area of briquettes under different compression loads.

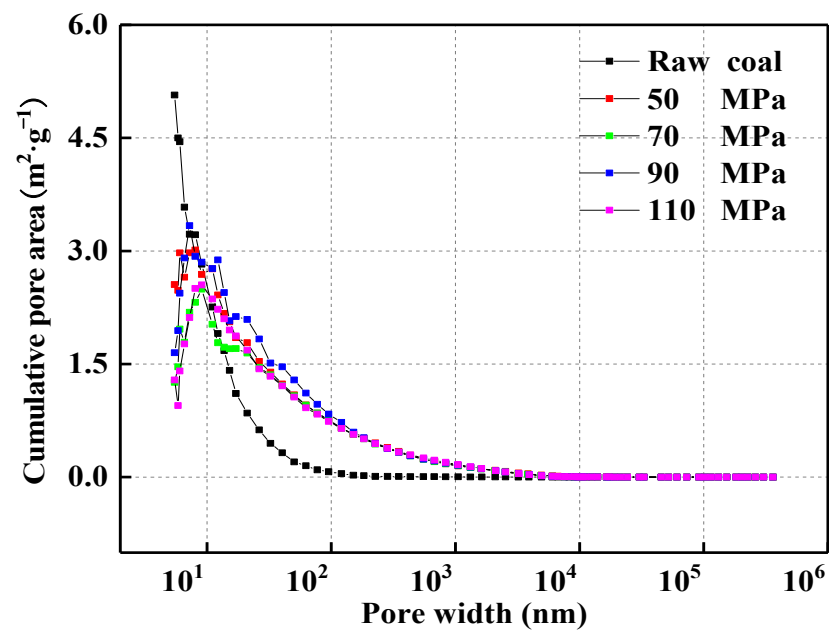


Figure 8. Cumulative pore area of briquettes under different compression loads.

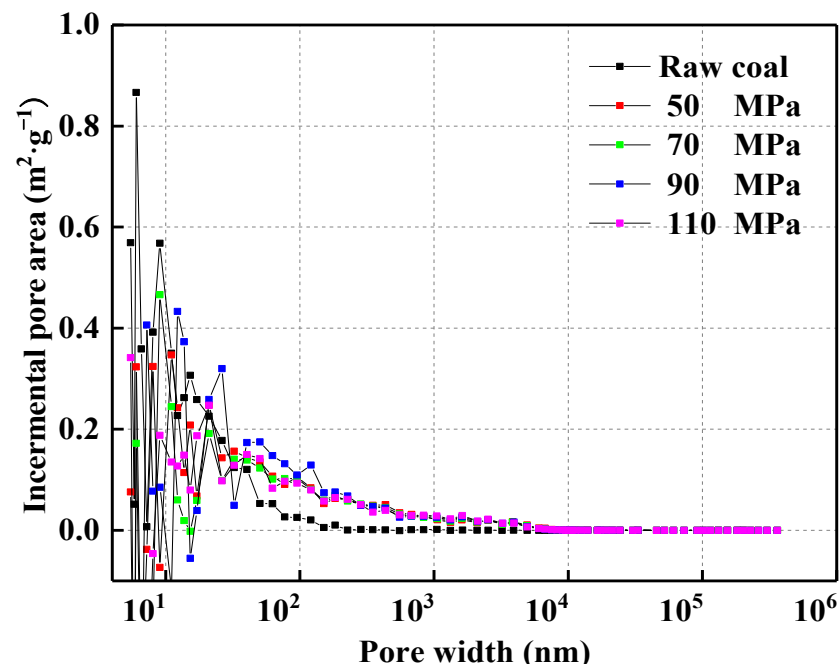


Figure 9. Incremental pore area of briquettes under different compression loads.

Table 2. Pore area distribution of briquettes under different compression loads.

Coal Sample	Pore area Distribution of Briquette with Different Compression Loads ($\text{m}^2 \cdot \text{g}^{-1}$)				
	<10 nm	10–10 ² nm	10 ² –10 ³ nm	10 ³ –10 ⁵ nm	>10 ⁵ nm
Raw coal	2.813	2.21	0.042	0.003	0.001
50 MPa	−0.208	2.11	0.505	0.148	0
70 MPa	−0.769	1.38	0.497	0.151	0
90 MPa	−1.116	2.041	0.568	0.158	0
110 MPa	−1.073	1.718	0.478	0.167	0

3.4. Fractal Characteristics of Pore Structure with Different Compression Loads of Briquette

In order to study the scale characteristics of the pore structure of briquette, we organize and analyze the experimental data of mercury intrusion of briquette samples according to the principle of fractal theory. When using mercury intrusion method to measure pore structure parameters, we derive the Washburn equation based on the principle of non-wetting capillary, and obtain the functional relationship between the mercury injection pressure and the pore size when the mercury injection is in equilibrium [36–40]:

$$p = -2\sigma\cos\beta/r \quad (1)$$

where p is the mercury injection pressure, MPa; σ is the surface tension of mercury, usually 0.485 N/m; β is the contact angle between mercury and coal wall, taking 130°; r is the pore size, nm.

According to Menger sponge model, the equation of porous medium dV/dp and fractal dimension D is established to analyze the fractal characteristics of pore structure. As follows:

$$\lg(dV/dp) \propto (D - 4)\lg p \quad (2)$$

where V is the mercury volume corresponding to the pressure p , cm^3/g ; D is the fractal dimension.

The mercury injection volume and the mercury injection pressure obtained from the mercury intrusion experiment are logarithmically processed to fit, according to Formula (2), there is a linear relationship between $\lg(dV/dp)$ and $\lg p$, that is, the relationship between fractal dimension D and slope K is obtained:

$$K = D - 4 \quad (3)$$

Fractal dimension is a method used to express the irregularity and complexity of porous media [41–44]. The fractal dimension is between 2 and 3. The fractal dimension is closer to 2, the smoother the pores, and the closer the fractal dimension is to 3, the more complex the pore structure and the rougher the surface [45–48].

Figure 10 is the fractal characteristic curve of pore structure obtained from the experimental data of mercury intrusion of briquette and raw coal. According to the different characteristics exhibited by the coordinates, the raw coal is fitted by two-stage method. The briquette with different compression loads is divided into three stages for fitting, which are defined as the low pressure section 1, the low pressure section 2, and the high pressure section 3. Among them, the low pressure section 1 corresponds to the larger effective width of pores and fissures, the low pressure section 2 corresponds to the effective width of medium and large pores, and the high pressure section 3 corresponds to the smaller effective width of pores. The fractal dimension data in Figure 10 are sorted and summarized, and the results are shown in Table 3. The fractal dimension D_1 of briquette with different compression loads is close to 2, D_2 is close to 3, and D_3 is greater than 3. The corresponding pore diameters at the boundary between the low pressure section 1 and the low pressure section 2 are 33,050.5–45,519.7 nm, and the corresponding pore diameters at the boundary between the low pressure section 2 and the high pressure section 3 are 26.3–40.3 nm. It shows that with the action of the applied load, the fractal characteristics of the low pressure section 1 of the briquette are similar to the raw coal, and the pore structure of briquette becomes complicated in the low pressure section 2, and the applied load changes the complexity and regularity of the pore structure of coal samples, and with the continuous increase of the mercury injection pressure, the tiny pores of the briquette are fractured, which does not conform to the fractal characteristics. The large-diameter pore structure of briquette with different compression loads is relatively simple, while the small-diameter pore structure are more complex, and the pore and fissure structure of briquette coal are more developed than that of raw coal.

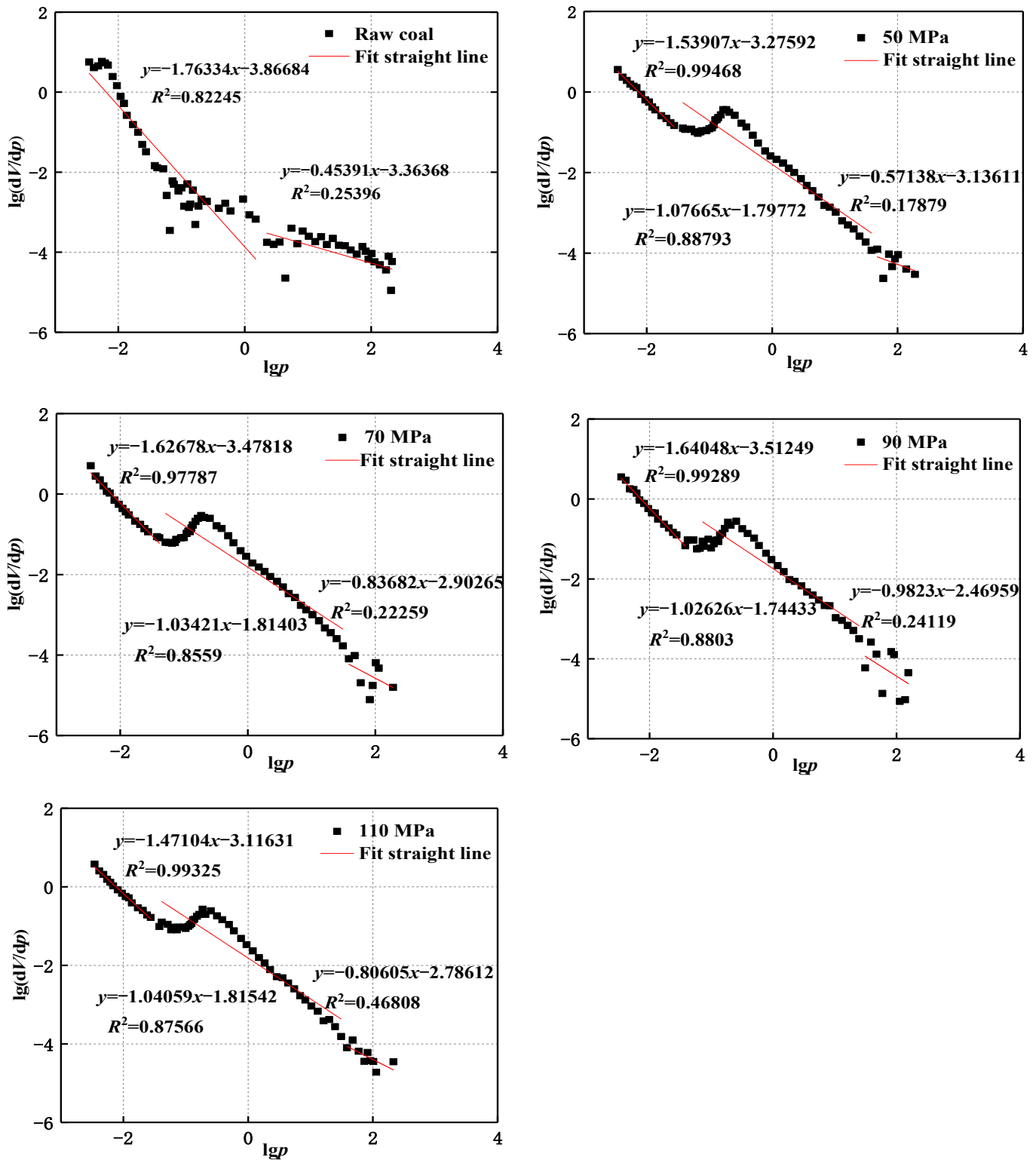


Figure 10. Characteristic curve of briquette type with different compression loads.

Table 3. Calculation results for the fractal dimensions of briquette pore structures under different compression loads.

	Coal Sample	Pore width (nm)	Slope K	D ₁	R ²
Low pressure section 1	Raw coal	>95.4 nm	−1.76334	2.23666	0.82245
	50 MPa	>45519.7 nm	−1.53907	2.46093	0.99468
	70 MPa	>33050.5 nm	−1.62678	2.37322	0.97787
	90 MPa	>33066.1 nm	−1.64048	2.35952	0.99289
	110 MPa	>45506.7 nm	−1.47104	2.52896	0.99325
Low pressure section 2	Coal sample	Pore width (nm)	Slope K	D ₂	R ²
	50 MPa	26.3–45,519.7 nm	−1.07665	2.92335	0.88793
	70 MPa	32.4–33,050.5 nm	−1.03421	2.96579	0.8559
	90 MPa	40.3–33,066.1 nm	−1.02626	2.97374	0.8803
	110 MPa	32.4–45,506.7 nm	−1.04059	2.95941	0.87566
High pressure section 3	Coal sample	Pore width (nm)	Slope K	D ₃	R ²
	Raw coal	5.5–95.4 nm	−0.4298	3.5702	0.6267
	50 MPa	<26.3 nm	−0.57138	3.42862	0.17879
	70 MPa	<32.4 nm	−0.83682	3.16318	0.22259
	90 MPa	<40.3 nm	−0.9823	3.0177	0.24119
110 MPa	<32.4 nm	−0.80605	3.19395	0.46808	

4. Conclusions

(1) During the mercury intrusion experiment, it is found that the pore connectivity of raw coal is better, while the pore connectivity of briquettes is poor. The pore-specific surface area of coal decreases from 5.069 m²/g to 1.259 m²/g, the total pore volume increases from 0.0553 cm³/g to 0.1877 cm³/g and the average pore size increases from 43.6 nm to 596.3 nm from the raw coal to briquettes loaded with a load of 70 MPa. When the compression load reaches 70 MPa, the intergranular pores of briquettes are compacted, and the specific surface area, total pore volume and average pore diameter do not change much with the load, remaining basically stable.

(2) The minipores, visible pores and fissures contribute 78% of the pore volume of raw coal, and the pore volume of briquettes is mainly provided by mesopores under the external load. The micropores and minipores of raw coal contribute 99% of the specific surface area, the pore area of the briquettes has more area contributed by mesopores and macropores compared with raw coal, and the surface area contributed by minipores is slightly reduced. The compression load has little effect on the pores of 10–100 nm, and the effect on the pores is mainly concentrated in the region of 100–10,000 nm.

(3) Combined with fractal theory, the results of mercury intrusion experiments are analyzed, and it is found that the pore structure of briquettes is relatively simple in low-pressure section 1, the pore structure of low-pressure section 2 is obviously complicated, and the pore structure of high-pressure section 3 is severely deformed or even collapsed due to the strong compression of the coal body from the increasing mercury injection pressure; section 3 does not have fractal characteristics. Furthermore, the applied load changes the complexity and regularity of the pore structure of the coal sample.

(4) The mercury intrusion method is used to test the pore structures of loaded briquettes, which are more likely to collapse and show damage to micropores (<10 nm). It is recommended to use other testing methods for micropores (<10 nm).

Author Contributions: Conceptualization, methodology and writing—original draft preparation, L.Q.; writing—review and editing, X.Z.; investigation, resources and data curation, X.P.; project administration and funding acquisition, X.C.; visualization and supervision, Z.W.; software, validation and formal analysis, J.D. All authors have read and agreed to the published version of the manuscript.

Funding: This research was funded by the National Natural Science Foundation of China (No. 51704100, No. 52074107, No. 52074105, No. 51874122); Postdoctoral Research Foundation of Henan Province (First-class financial support); Henan Provincial Key Laboratory of Gas Geology and Gas

Control - Open Project of the State Key Laboratory Cultivation Base jointly built by the province and the ministry (No. WS2018B13, No. WS2020B14); Doctoral Fund of Henan Polytechnic University (No. B2016-004); Fundamental and Frontier Technology Research Project of Henan Province (No. 162300410038); Key Scientific Research Project of Higher Education Institutions of Henan Provincial Department of Education (No. 15A440007).

Institutional Review Board Statement: Not applicable.

Informed Consent Statement: Not applicable.

Data Availability Statement: The data used to support the findings of this study are available from the corresponding author upon reasonable request.

Conflicts of Interest: All authors declare no competing interests in this study.

References

- Zhao, Z.; Chang, P.; Xu, G.; Ghosh, A.; Li, D.; Huang, J. Comparison of the Coal Dust Suppression Performance of Surfactants Using Static Test and Dynamic Test. *J. Clean. Prod.* **2021**, *328*, 129633. [[CrossRef](#)]
- Gao, D.; Hong, L.; Wang, J.; Zheng, D. Molecular Simulation of Gas Adsorption Characteristics and Diffusion in Micropores of Lignite. *Fuel* **2020**, *269*, 117443. [[CrossRef](#)]
- Xu, J.; Ye, G.; Li, B.; Cao, J.; Zhang, M. Experimental Study of Mechanical and Permeability Characteristics of Moulded Coals with Different Binder Ratios. *Rock Soil Mech.* **2015**, *36*, 104–110. [[CrossRef](#)]
- Cao, J.; Sun, H.; Wang, B.; Dai, L.; Zhao, B.; Wen, G.; Zhao, X. A Novel Large-Scale Three-Dimensional Apparatus to Study Mechanisms of Coal and Gas Outburst. *Int. J. Rock Mech. Min. Sci.* **2019**, *118*, 52–62. [[CrossRef](#)]
- Cabalar, A.F.; Alosman, S.O. Influence of Rock Powder on the Behaviour of an Organic Soil. *Bull. Eng. Geol. Environ.* **2021**, *80*, 8665–8676. [[CrossRef](#)]
- Premkumar, S.; Piratheepan, J.; Rajeev, P.; Arulrajah, A. Stabilizing Dispersive Soil Using Brown Coal Fly Ash and Hydrated Lime. In Proceedings of the Geo-Chicago 2016, Chicago, IL, USA, 14–18 August 2016; American Society of Civil Engineers: Reston VA, USA, 2016; pp. 874–884.
- Minitiskii, A.V.; Loboda, P.I. The Infiltration of Lubricants into a Porous Briquette, When Compacting. *Powder Metall. Met. Ceram.* **2017**, *55*, 640–643. [[CrossRef](#)]
- Sun, L.; Jia, N.; Yang, X. Relationship between Pore Structure and Gas Permeability of Raw Coal and Briquette Coal. *Saf. Coal Mines* **2022**, *53*, 24–30. [[CrossRef](#)]
- Jia, H.; Wang, K.; Wang, Y.; Sun, X. Permeability Characteristics of Gas-Bearing Coal Specimens under Cyclic Loading-Unloading of Confining Pressure. *J. China Coal Soc.* **2020**, *45*, 1710–1718. [[CrossRef](#)]
- Ma, J.; Hou, C.; Xin, C.; Li, J. Experimental Study on Permeability Characteristics of Briquette Coal after Peak. *J. Saf. Sci. Technol.* **2017**, *13*, 104–109.
- Li, X.; Wang, Z.; Qi, C.; Yue, G. Freezing Experiments on Moulded Coal with Methane Using Dry Ice as Cold Source. *J. China Coal Soc.* **2017**, *42*, 160–165. [[CrossRef](#)]
- Wang, Z.; Wang, L.; Dong, J.; Wang, Q. Simulation on the Temperature Evolution Law of Coal Containing Gas in the Freezing Coring Process. *J. China Coal Soc.* **2021**, *46*, 199–210. [[CrossRef](#)]
- Wang, Q.; Wang, Z.; Ma, S.; Zhang, K. Study on Temperature Variation of Coal Sample in Process of Freezing Coring. *China Saf. Sci. J.* **2021**, *31*, 76–81. [[CrossRef](#)]
- Zhang, Z.; Chen, Y.; Zhao, D.; Tang, C.; Ma, K.; Zhang, C. Comparative Study of Adsorption/Desorption and Deformation Characteristics of Raw and Briquette Coals under CO₂. *J. China Univ. Min. Technol.* **2021**, *50*, 793–803. [[CrossRef](#)]
- Zhou, A.; Du, C.; Wang, K.; Hu, J.; Fan, X. Experimental Research on the Law of the Deformation and Damage Characteristics of Raw Coal/ Briquette Adsorption-Instantaneous Pressure Relief. *Fuel* **2022**, *308*, 122062. [[CrossRef](#)]
- Nie, B.; Hu, S.; Li, X.; Zhai, S.; Meng, J. Experimental Study of Deformation Rules during the Process of Gas Adsorption and Desorption in Briquette Coal. *Int. J. Min. Reclam. Environ.* **2014**, *28*, 277–286. [[CrossRef](#)]
- Wang, H.; Li, Q.; Yuan, L.; Li, S.; Xue, J.; Zhu, H.; Duan, R.; Wang, S. Similar Material Research and Property Analysis of Coal Briquette in Coal and Gas Outburst Simulation Test. *J. Min. Saf. Eng.* **2018**, *35*, 1277–1283. [[CrossRef](#)]
- Yin, Y.; Zhang, X.; Jiang, F.; Yu, Z. Study on Mechanical Mechanism and Danger Evaluation Technology of Coal and Gas Outburst Induced by Rockburst. *J. Min. Saf. Eng.* **2018**, *35*, 801–809. [[CrossRef](#)]
- Gan, Q.; Xu, J.; Peng, S.; Yan, F.; Wang, R.; Cai, G. Effects of Heating Temperature on Pore Structure Evolution of Briquette Coals. *Fuel* **2021**, *296*, 120651. [[CrossRef](#)]
- Zhao, Y.; Zhang, Y.; Zhang, H.; Wang, Q.; Guo, Y. Structural Characterization of Carbonized Briquette Obtained from Anthracite Powder. *J. Anal. Appl. Pyrolysis* **2015**, *112*, 290–297. [[CrossRef](#)]
- Skoczylas, N.; Dutka, B.; Sobczyk, J. Mechanical and Gaseous Properties of Coal Briquettes in Terms of Outburst Risk. *Fuel* **2014**, *134*, 45–52. [[CrossRef](#)]
- Li, S.; Zhang, X.; Yan, M.; Bai, Y. Effect of Coal Particle Size on Pore Structure Characteristic and Gas Adsorption Characteristic. *Min. Saf. Environ. Prot.* **2019**, *46*, 8–12.

23. Xu, J.; Lu, Q.; Wu, X.; Liu, D. The Fractal Characteristics of the Pore and Development of Briquettes with Different Coal Particle Sizes. *J. Chongqing Univ.* **2011**, *34*, 81–89.
24. Zhang, H. Evaluation and Prevention of Mining Subsidence in Coal Mines. *Coal Min. Technol.* **2015**, *20*, 1–2. [[CrossRef](#)]
25. Gao, D.; Hong, L.; Wang, J.; Zheng, D. Adsorption Simulation of Methane on Coals with Different Metamorphic Grades. *AIP Adv.* **2019**, *9*, 095108. [[CrossRef](#)]
26. Wang, K.; Zang, J.; Feng, Y.; Wu, Y. Effects of Moisture on Diffusion Kinetics in Chinese Coals during Methane Desorption. *J. Nat. Gas Sci. Eng.* **2014**, *21*, 1005–1014. [[CrossRef](#)]
27. Mou, P.; Pan, J.; Niu, Q.; Wang, Z.; Li, Y.; Song, D. Coal Pores: Methods, Types, and Characteristics. *Energy Fuels* **2021**, *35*, 7467–7484. [[CrossRef](#)]
28. Chang, P.; Xu, G.; Chen, Y.; Ghosh, A.; Moridi, M.A. Improving Coal Powder Wettability Using Electrolyte Assisted Surfactant Solution. *Colloids Surf. A Physicochem. Eng. Asp.* **2021**, *613*, 126042. [[CrossRef](#)]
29. He, Q.; Zhu, L.; Li, Y.; Li, D.; Zhang, B. Simulating Hydraulic Fracture Re-Orientation in Heterogeneous Rocks with an Improved Discrete Element Method. *Rock Mech. Rock Eng.* **2021**, *54*, 2859–2879. [[CrossRef](#)]
30. Hao, Q. On Morphological Character and Origin of Micropores in Coal. *J. China Coal Soc.* **1987**, *4*, 51–56. [[CrossRef](#)]
31. Wu, J.; Jin, K.; Tong, Y.; Qian, R. Theory of Coal Pores and its Application in Evaluation of Gas Outburst Proneness. *J. China Coal Soc.* **1991**, *16*, 86–95. [[CrossRef](#)]
32. Zhu, J.; Yang, Y.; Shao, T.; Hou, C.; Jiang, Y.; Zhao, Y.; Wang, J.; Li, J. Pore Size Distributions and Multi-Fractal Characteristics of the Intact and Pulverized Coal in High Gas Mine. *Geotech. Geol. Eng.* **2022**, *40*, 4943–4959. [[CrossRef](#)]
33. Liu, J.; Ma, J.; Jiang, X.; Jiang, X. The Multi-Scale Pore Structure of Superfine Pulverized Coal. Part 1. Macropore Morphology. *Fuel* **2021**, *304*, 120728. [[CrossRef](#)]
34. Zhang, J.; Li, X.; Jiao, J.; Liu, J.; Chen, F.; Song, Z. Comparative Study of Pore Structure Characteristics between Mudstone and Coal under Different Particle Size Conditions. *Energies* **2021**, *14*, 8435. [[CrossRef](#)]
35. Qi, L.; Zhou, X.; Peng, X.; Wang, Z.; Dai, J. Study on pore structure of coking coal based on low-temperature nitrogen adsorption and mercury intrusion method. *Saf. Coal Mines* **2022**, *53*, 1–6. [[CrossRef](#)]
36. Zhang, M.; Duan, C.; Li, G.; Fu, X.; Zhong, Q.; Liu, H.; Dong, Z. Determinations of the Multifractal Characteristics of the Pore Structures of Low-, Middle-, and High-Rank Coal Using High-Pressure Mercury Injection. *J. Pet. Sci. Eng.* **2021**, *203*, 108656. [[CrossRef](#)]
37. Wang, J.; Jiang, F.; Zhang, C.; Song, Z.; Mo, W. Study on the Pore Structure and Fractal Dimension of Tight Sandstone in Coal Measures. *Energy Fuels* **2021**, *35*, 3887–3898. [[CrossRef](#)]
38. Zhao, Z.; Ni, X.; Cao, Y.; Shi, Y. Application of Fractal Theory to Predict the Coal Permeability of Multi-Scale Pores and Fractures. *Energy Rep.* **2021**, *7*, 10–18. [[CrossRef](#)]
39. Zhao, S.; Chen, X.; Li, X.; Qi, L.; Zhang, G. Experimental Analysis of the Effect of Temperature on Coal Pore Structure Transformation. *Fuel* **2021**, *305*, 121613. [[CrossRef](#)]
40. Xu, Y.; Chen, X.; Zhao, W.; Chen, P. Effect of Water Intrusion on the Characteristics of Surface Morphology and Pore Fracture Spaces in Argillaceous Meagre Coal. *J. Nat. Gas Sci. Eng.* **2020**, *81*, 103404. [[CrossRef](#)]
41. Lu, G.; Wang, J.; Wei, C.; Song, Y.; Yan, G.; Zhang, J.; Chen, G. Pore Fractal Model Applicability and Fractal Characteristics of Seepage and Adsorption Pores in Middle Rank Tectonic Deformed Coals from the Huaibei Coal Field. *J. Pet. Sci. Eng.* **2018**, *171*, 808–817. [[CrossRef](#)]
42. Ren, W.; Zhou, H.; Zhong, J.; Xue, D.; Wang, C.; Liu, Z. A Multi-Scale Fractal Approach for Coal Permeability Estimation via MIP and NMR Methods. *Energies* **2022**, *15*, 2807. [[CrossRef](#)]
43. Zhu, J.; Shao, T.; Li, G.; Yang, Y.; Chen, Z.; Lan, T.; Wang, J.; Zhao, Y.; Liu, S. Multiscale Pore Structure Characteristics and Crack Propagation Behavior of Coal Samples from High Gas Seam. *Materials* **2022**, *15*, 4500. [[CrossRef](#)] [[PubMed](#)]
44. Ren, J.; Wang, Z.; Li, B.; Chen, F.; Liu, J.; Liu, G.; Song, Z. Fractal-Time-Dependent Fick Diffusion Model of Coal Particles Based on Desorption–Diffusion Experiments. *Energy Fuels* **2022**, *36*, 6198–6215. [[CrossRef](#)]
45. Li, C.; Yao, H.; Xin, C.; Li, H.; Guan, J.; Liu, Y. Changes in Pore Structure and Permeability of Middle–High Rank Coal Subjected to Liquid Nitrogen Freeze–Thaw. *Energy Fuels* **2021**, *35*, 226–236. [[CrossRef](#)]
46. Zhang, K.; Cheng, Y.; Wang, L.; Dong, J.; Hao, C.; Jiang, J. Pore Morphology Characterization and Its Effect on Methane Desorption in Water-Containing Coal: An Exploratory Study on the Mechanism of Gas Migration in Water-Injected Coal Seam. *J. Nat. Gas Sci. Eng.* **2020**, *75*, 103152. [[CrossRef](#)]
47. Hu, Y.; Guo, Y.; Shangguan, J.; Zhang, J.; Song, Y. Fractal Characteristics and Model Applicability for Pores in Tight Gas Sandstone Reservoirs: A Case Study of the Upper Paleozoic in Ordos Basin. *Energy Fuels* **2020**, *34*, 16059–16072. [[CrossRef](#)]
48. Ye, Z.; Hou, E.; Duan, Z. Micrometer-Scale Pores and Fractures in Coals and the Effects of Tectonic Deformation on Permeability Based on Fractal Theory. *AIP Adv.* **2020**, *10*, 025118. [[CrossRef](#)]